



UNIVERSITY OF LEEDS

This is a repository copy of *Terahertz master-oscillator power-amplifier quantum Cascade laser with controllable polarization*.

White Rose Research Online URL for this paper:

<https://eprints.whiterose.ac.uk/163358/>

Version: Supplemental Material

---

**Article:**

Zhu, H, Zhu, H, Wang, K et al. (9 more authors) (2020) Terahertz master-oscillator power-amplifier quantum Cascade laser with controllable polarization. *Applied Physics Letters*, 117 (2). 021103. ISSN 0003-6951

<https://doi.org/10.1063/5.0013505>

---

This article may be downloaded for personal use only. Any other use requires prior permission of the author and AIP Publishing. This article appeared in Zhu, H. et al (2020). Terahertz master-oscillator power-amplifier quantum Cascade laser with controllable polarization. *App. Phys. Letters*, 117(2), 021103 and may be found at <https://doi.org/10.1063/5.0013505>

**Reuse**

Items deposited in White Rose Research Online are protected by copyright, with all rights reserved unless indicated otherwise. They may be downloaded and/or printed for private study, or other acts as permitted by national copyright laws. The publisher or other rights holders may allow further reproduction and re-use of the full text version. This is indicated by the licence information on the White Rose Research Online record for the item.

**Takedown**

If you consider content in White Rose Research Online to be in breach of UK law, please notify us by emailing [eprints@whiterose.ac.uk](mailto:eprints@whiterose.ac.uk) including the URL of the record and the reason for the withdrawal request.

# Terahertz master-oscillator power-amplifier quantum cascade laser with controllable polarization: Supplementary Material

Haiqing Zhu,<sup>1,2</sup> Huan Zhu,<sup>1</sup> Kai Wang,<sup>1</sup> Chenren Yu,<sup>1,2</sup> Gaolei Chang,<sup>1,2</sup> Fangfang Wang,<sup>1</sup> Jianxin Chen,<sup>1</sup> Lianhe Li,<sup>3</sup> A. Giles Davies,<sup>3</sup> Edmund H. Linfield,<sup>3</sup> Gangyi Xu,<sup>1,4\*</sup> and Li He<sup>1</sup>

<sup>1</sup>Key Laboratory of Infrared Imaging Materials and Detectors, Shanghai Institute of Technical Physics, Chinese Academy of Sciences, Shanghai 200083, China

<sup>2</sup>University of Chinese Academy of Sciences, Beijing 100049, China

<sup>3</sup> School of Electronic and Electrical Engineering, University of Leeds, Leeds LS2 9JT, United Kingdom

<sup>4</sup> Hangzhou Institute for Advanced Study, UCAS, Hangzhou 310024, China

\*Author e-mail address: gangyi.xu@mail.sitp.ac.cn

## 1. Structure parameters of the THz-MOPA-QCLs

Figure S1 gives SEM pictures of MOPA devices with the first type and the second type of the antenna array. The DFB grating contains 80 periods with a central  $\pi$  phase shift. The width, the duty cycle and the groove etch depth of the grating are 280  $\mu\text{m}$ , 60% and 450 nm, respectively. The straight preamplifier is 500  $\mu\text{m}$ -long. The antenna arrays contain 9  $\times$  15 unit cells. The lateral periodicity ( $P_y$ ) of the 2D antenna arrays is 23  $\mu\text{m}$ . The longitudinal periodicities ( $P_x$ ) are 37  $\mu\text{m}$  for the first type array and 35  $\mu\text{m}$  for the second type array, respectively. The size of the antennas is 16  $\mu\text{m} \times$  7  $\mu\text{m}$ .

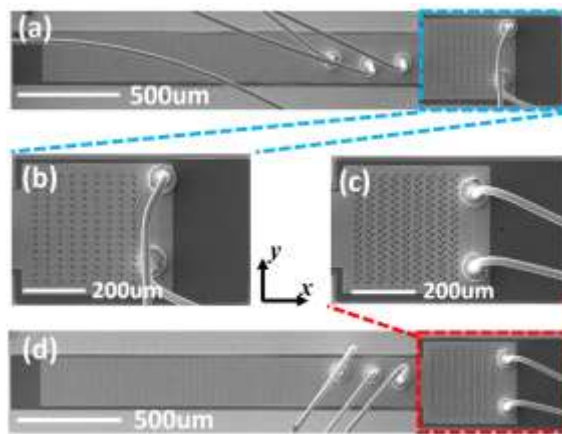


**FIG. S1 SEM pictures of the MOPA devices with the 2D antenna array.** Panels (a) and (b) show the device with the first type of the antenna array, in which the orientation angle of the antennas is 45° with respect to the x-direction. Panels (c) and (d) show the device with the second type of the antenna array, in which the two sub-arrays have orthogonal orientations. The longitudinal interval  $S_x$  and the lateral interval  $S_y$  are respectively 12  $\mu\text{m}$  and 11.5  $\mu\text{m}$ .

## 2. Degree of the linear polarization (DOLP)

The Stokes parameters  $s_0$ ,  $s_1$ ,  $s_2$  and  $s_3$  are usually utilized to describe the polarization state, where  $s_0 = a_1^2 + a_2^2$ ,  $s_1 = a_1^2 - a_2^2$ ,  $s_2 = 2a_1a_2 \cos \delta$  and  $s_3 = 2a_1a_2 \sin \delta$ . Here,  $a_1$  and  $a_2$  are respectively the amplitude of orthogonal electric vectors, and  $\delta$  is the phase difference between them.

The degree of linear polarization is defined as  $DOLP = \sqrt{s_1^2 + s_2^2}/s_0$ , and the polarization azimuth equals to  $\tan 2\theta_P = s_2/s_1$ . The Stokes parameters can be calculated by the power  $I(\alpha)$  through a polarizer versus the orientation angle  $\alpha$ , where  $s_0 = I(0^\circ) + I(90^\circ)$ ,  $s_1 = I(0^\circ) - I(90^\circ)$  and  $s_2 = I(45^\circ) - I(135^\circ)$ . For the first type of antenna array, the polarization ellipse of the radiation calculated by the 3D FDTD method is shown in Fig. 1(e). The normalized power is therefore calculated (shown in Fig. S2), from which the DOLP is found to be 99.9% and the polarization azimuth ( $\theta_P$ ) is  $-28^\circ$ .

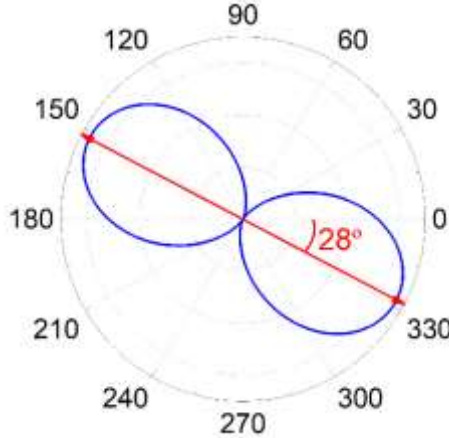


**FIG. S2. Normalized power through a polarizer as a function of its orientation angle  $\alpha$ , calculated for the radiation at the brightness point on the beam pattern. The angle  $\alpha = 0^\circ$  responds to  $+x$ -direction.**

## 3. Comparison of the beam divergence and the diffraction limit

The divergent angle of the single-lobed beam (full width at half maximum, FWHM) is approximately  $20^\circ \times 28^\circ$ , as shown in Fig. 2(c). The angular definition of the far-field measurement is given in Fig. S3(a). The size of the 2D antenna array is  $\sim 360 \mu\text{m} \times 370 \mu\text{m}$ , so the corresponding diffraction limit is  $\sim 20^\circ \times 20^\circ$ . As shown in Fig. S3(b), the field spread covers the whole antenna array along the  $x$ -direction, which makes the divergent angle along the  $\theta_x$  direction close to the diffraction limit. On the other hand, the antenna array is wider than the preamplifier and the field expansion is unobvious when the THz wave is injected from the preamplifier into the antenna array, therefore the field spread is less than the width of the antenna array ( $y$ -direction). As a result, the divergent angle along the  $\theta_y$  direction is larger than the diffraction limit. Figure S3(b) shows that the effective size of the emission surface in  $y$ -direction is close to the width of the

preamplifier (280  $\mu\text{m}$ ). Take this into account, the measured divergent angle is close to the diffraction limit.

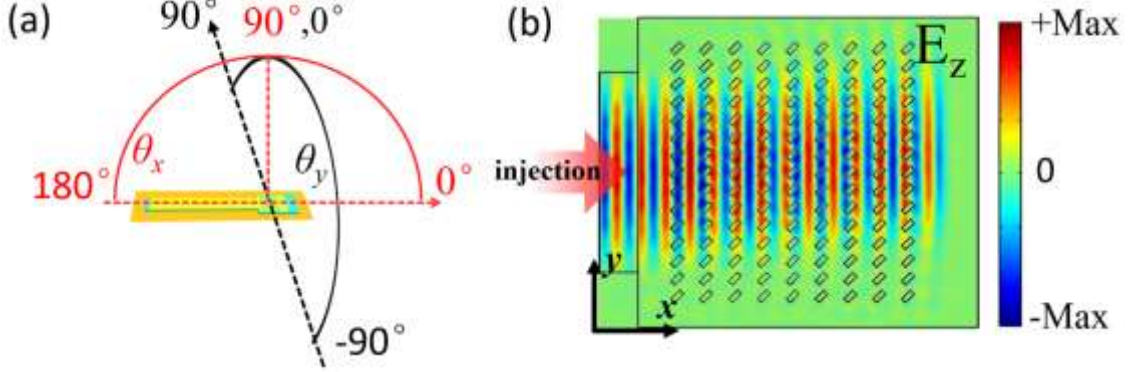


**FIG. S3** (a) Angular definition of the far-field measurement, in which the angle  $\theta_x = \theta_y = 0^\circ$  corresponds to the direction along the laser ridge. (b) Normalized electric field distribution ( $E_z$ ) in the antenna array in an  $x$ - $y$  plane across the center of the active region.

#### 4. Degree of the circular polarization (DOCP)

The electric field  $\vec{E}$  at the diffraction direction ( $\theta_x=\beta$ ,  $\theta_y=0$ ), as described in Eq. (1), can be decomposed into components along the  $x$ - and  $y$ -direction ( $E_x$  and  $E_y$ ), as the following

$$\begin{aligned} E_x &= A_0 \cos \frac{\theta_{pol}}{2} [\cos \omega_0 t + \cos(\omega_0 t + \Delta \Phi_e)] \\ &= 2A_0 \cos \frac{\theta_{pol}}{2} \cos \frac{\Delta \Phi_e}{2} \cos \left( \omega_0 t + \frac{\Delta \Phi_e}{2} \right), \end{aligned} \quad (\text{S1})$$

$$\begin{aligned} E_y &= A_0 \sin \frac{\theta_{pol}}{2} [\cos \omega_0 t - \cos(\omega_0 t + \Delta \Phi_e)] \\ &= 2A_0 \sin \frac{\theta_{pol}}{2} \sin \frac{\Delta \Phi_e}{2} \cos \left( \omega_0 t + \frac{\Delta \Phi_e}{2} - \frac{\pi}{2} \right). \end{aligned} \quad (\text{S2})$$

The phase difference  $\delta$  between  $E_x$  and  $E_y$  is  $-\pi/2$ , and the amplitudes of these two orthogonal electric vectors ( $a_1$  and  $a_2$ ) read

$$a_1 = 2A_0 \cos \frac{\theta_{pol}}{2} \cos \frac{\Delta \Phi_e}{2}, \quad (\text{S3})$$

$$a_2 = 2A_0 \sin \frac{\theta_{pol}}{2} \sin \frac{\Delta \Phi_e}{2}. \quad (\text{S4})$$

The degree of circular polarization is defined as  $|s_3/s_0|$ , where the Stork parameters equal to  $s_0 = a_1^2 +$

$a_2^2$  and  $s_3 = -2a_1a_2$ . Therefore, the DOCP is given by

$$\text{DOCP} = \left| 2a_1a_2/(a_1^2 + a_2^2) \right| = \left| \frac{\sin(\Delta\Phi_e)\sin(\theta_{pol})}{2\sin^2(\frac{\Delta\Phi_e}{2})\sin^2(\frac{\theta_{pol}}{2})+2\cos^2(\frac{\Delta\Phi_e}{2})\cos^2(\frac{\theta_{pol}}{2})} \right|. \quad (\text{S5})$$

Obviously, a circularly polarized beam (DOCP = 100%) is obtained when  $\Delta\Phi_e + \theta_{pol} = \pi$ . Experimentally,  $a_1$  and  $a_2$  correspond to  $I_{max}^{1/2}$  and  $I_{min}^{1/2}$ , and the DOCP is  $2\sqrt{I_{max}I_{min}}/(I_{max} + I_{min})$ , where  $I_{max}$  and  $I_{min}$  are the maximum and the minimum power through a polarizer when its orientation rotates.

##### 5. Estimation of the power amplification of the MOPA configuration

The THz power generated in the DFB laser is amplified in the preamplifier and is extracted into free space by the 2D antenna array. We have fabricated and compared two MOPA devices with or without a preamplifier, in which the DFB section and the 2D antenna array ( $S_x = 9 \mu\text{m}$ ) are the same. Fig. S4 shows the light-current density curves of these two devices, in which the red curve corresponds to the device without a preamplifier, while the black curve corresponds to the device with a 500  $\mu\text{m}$ -long preamplifier. Both of them measured at 20 K under the same conditions. Figure S4 shows that, with a preamplifier the THz power from the DFB laser is amplified by a factor of  $\sim 1.7$ .

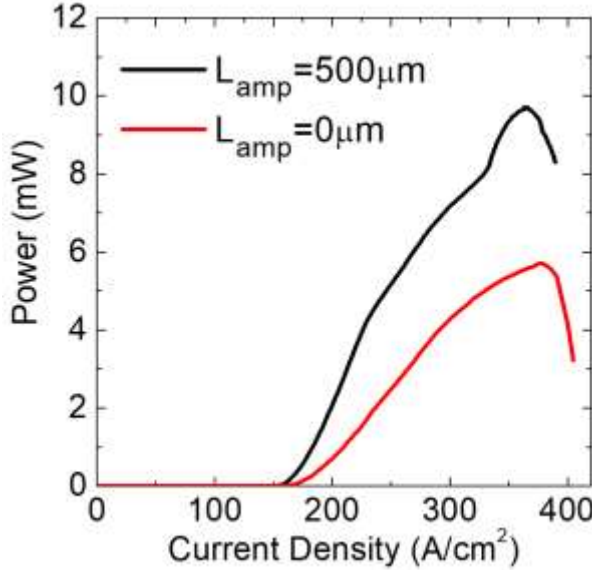


**FIG. S4** Light-current density ( $L$ - $J$ ) curves of two devices with the same DFB structure and 2D antenna array but different values of  $L_{amp}$  (0  $\mu\text{m}$  and 500  $\mu\text{m}$ ), measured at 20 K in pulsed mode.

##### 6. The non-uniformity of the polarization for the devices with the second-type of antenna array

For two devices with the second type of antenna array ( $S_x = 9 \mu\text{m}$  and 12  $\mu\text{m}$ , respectively), Figs. 4(e)

and 4(f) show the measured THz power versus the orientation angle of the polarizer at different spots on the related beam patterns. Here, in Table S1, at these spots we list the simulated and measured values of DOCP. When  $S_x = 9 \mu\text{m}$ , the simulated DOCP varies from 66.4% to 84.2%, and the measured results agree reasonably with the calculations except the Spot E. When  $S_x = 12 \mu\text{m}$ , the simulated DOCP varies from 98.3% to 99.9%, while the measured DOCP changes from 90.6% to 99.3%, indicating a good agreement.

**TABLE S1. Simulated and measured values of DOCP at different spots on the beam patterns.**

Device with $S_x = 9 \mu\text{m}$			Device with $S_x = 12 \mu\text{m}$		
Spot	Simulated DOCP	Measured DOCP	Spot	Simulated DOCP	Measured DOCP
A	75.8%	76.8%	A	99.9%	99.3%
B	84.2%	84.7%	B	99.5%	99.8%
C	77.8%	77.4%	C	98.6%	96.4%
D	66.4%	65.1%	D	98.3%	90.6%
E	75.7%	55.9%	E	98.9%	95.1%